Asian Spine Journal
Basic Study
Asian Spine J 2022;16(5):615-624 • https://doi.org/10.31616/asj.2021.0424

Biomechanical Study of Cervical Endplate Removal on Subsidence and Migration in Multilevel Anterior Cervical Discectomy and Fusion

Maohua Lin[1], Rudy Paul[1], Stephen Z. Shapiro[2], James Doulgeris[2], Timothy E. O'Connor[3], Chi-Tay Tsai[1], Frank D. Vrionis[2]

[1]*Department of Ocean and Mechanical Engineering, Florida Atlantic University, Boca Raton, FL, USA*
[2]*Department of Neurosurgery, Marcus Neuroscience Institute, Boca Raton Regional Hospital, Boca Raton, FL, USA*
[3]*Department of Neurosurgery, Jacobs School of Medicine and Biomedical Sciences, University at Buffalo, Buffalo, NY, USA*

Study Design: This study compares four cervical endplate removal procedures, validated by finite element models.

Purpose: To characterize the effect of biomechanical strength and increased contact area on the maximum von Mises stress, migration, and subsidence between the cancellous bone, endplate, and implanted cage.

Overview of Literature: Anterior cervical discectomy and fusion (ACDF) has been widely used for treating patients with degenerative spondylosis. However, no direct correlations have been drawn that incorporate the impact of the contact area between the cage and the vertebra/endplate.

Methods: Model 1 (M1) was an intact C2C6 model with a 0.5 mm endplate. In model 2 (M2), a cage was implanted after removal of the C4–C5 and C5–C6 discs with preservation of the osseous endplate. In model 3 (M3), 1 mm of the osseous endplate was removed at the upper endplate. Model 4 (M4) resembles M3, except that 3 mm of the osseous endplate was removed.

Results: The range of motion (ROM) at C2C6 in the M2–M4 models was reduced by at least 9° compared to the M1 model. The von Mises stress results in the C2C3 and C3C4 interbody discs were significantly smaller in the M1 model and slightly increased in the M2–M3 and M3–M4 models. Migration and subsidence decreased from the M2–M3 model, whereas further endplate removal increased the migration and subsidence as shown in the transition from M3 to M4.

Conclusions: The M3 model had the least subsidence and migration. The ROM was higher in the M3 model than the M2 and M4 models. Endplate preparation created small stress differences in the healthy intervertebral discs above the ACDF site. A 1 mm embedding depth created the best balance of mechanical strength and contact area, resulting in the most favorable stability of the construct.

Keywords: Cervical spine; Anterior cervical discectomy and fusion; Finite element analysis; Migration; Subsidence

Introduction

Anterior cervical discectomy and fusion (ACDF) is a common procedure involving the removal of the intervertebral disc [1]. Subsidence and migration commonly arise in the early postoperative stages. These may then cause fo-

Received Oct 18, 2021; Accepted Nov 14, 2021
Corresponding author: Frank D. Vrionis
Department of Neurosurgery, Marcus Neuroscience Institute, Boca Raton Regional Hospital, 800 Meadows Road, Boca Raton, Florida, 33486, USA
Tel: +1-561-955-5977, Fax: +1-561-955-3259, E-mail: FVrionis@baptisthealth.net

ASJ
Copyright © 2022 by Korean Society of Spine Surgery
This is an Open Access article distributed under the terms of the Creative Commons Attribution Non-Commercial License (http://creativecommons.org/licenses/by-nc/4.0/) which permits unrestricted non-commercial use, distribution, and reproduction in any medium, provided the original work is properly cited.

raminal stenosis [2], misalignment of the spine [3,4], and eventual mechanical failure at either the screw-plate/cage or the screw–vertebra interface, manifesting as pain and cervical radiculopathy [5]. Subsidence occurs when significant loads are applied at the contact of two materials with vastly different mechanical strengths [6]. Literature reports that bone mineral density and endplate thickness are proportional to the failure load of the structure [7]. Given this information, reduction of the endplates should likely result in higher failure rates or at least greater subsidence and migration [8]. Short-term issues of stability, misalignment, and higher rates of pseudarthrosis in multilevel fusions pose a case for endplate preservation. This would better distribute the loading and therefore reduce the load at the cage–vertebrae contact surface [9,10].

Some studies detail the effects of endplate geometry and mechanical properties on stability, alignment, and pseudarthrosis. However, these studies rarely combine such properties with the inclusion of the underlying vertebra and the impact it may have on load bearing and migration (sliding of the cage along the surface of the vertebra) [11]. One biomechanical mechanism for relatively high fusion rates with standalone cervical interbody may be the reduction of stress shielding from the elimination of the anterior plate and an increase in compressive forces described by Wolff's law [12]. Literature generally considers cage distraction a minute issue in the long term due to minimal patient discomfort and comparable fusion success rates [13]. These short-term issues of stability and misalignment and resulting problems combined with some fusion failures establish a case for the inclusion of exterior support methods to re-distribute and reduce the load at the cage–vertebra contact surface.

Few studies have emphasized the impact of the underlying cancellous bone contact with respect to handling large loads from the cage [14]. This study seeks to quantify the subsidence and migration of the cage as it is embedded further into the vertebra. This will be contrasted with the resulting stresses present in the upper-level vertebra to facilitate discussion of the benefits and consequences of endplate removal and embedding of the cage. To achieve this goal, a C2C6 model was developed without the inclusion of an anterior plating to reduce the load distribution and encourage a moderate amount of subsidence at the ACDF site. The C2C3 and C3C4 intervertebral discs were prioritized over C6C7 because there is a tendency for adjacent segment disease (ASD) to develop in the interbody levels above the indexed location of ACDF surgery [15].

Materials and Methods

1. Models

CT scans were analyzed and stitched into three-dimensional (3D) models of a healthy spine. The model was further edited and refined using the Mimics program (Materialise, Leuven, Belgium). The cages were designed and implemented into the finalized C2C6 model using SolidWorks 2019 (Dassault Systèmes SolidWorks Corp., Waltham, MA, USA). The model from a patient was imported into the ANSYS Workbench (ANSYS Inc., Canonsburg, PA, USA) and edited to create four separate models. The vertebra was divided into the cortical bone, modeled as a shell element of 0.2 mm thickness, and the cancellous bone, modeled as a solid body with tetrahedral elements. The endplates were modeled according to literature with a thickness of 0.5 mm with solid hexahedron elements [1]. The intervertebral discs were composed of the nucleus pulposus and annular ground, both with solid hexahedron elements. Five different cervical spine ligaments were included as nonlinear spring elements: anterior longitudinal (ALL), posterior longitudinal (PLL), ligamentum flavum, interspinous, and capsular ligaments. All cervical instrumentation, including the cages, plating, and screws, was modeled with tetrahedral elements.

Model 1 consisted of the intact C2C6 model with no implanted cages (Fig. 1A). Model 2 had an implanted cage with a height of 3 mm, equivalent to the disc height at the C4C5 and C5C6 sites where discectomy was performed. The cage was implanted with minimal endplate preparation (Fig. 1C). The model 3 procedure increased the cage height to 4 mm. The contact with the lower endplate remained the same. The upper endplate and vertebra were removed to embed the cage 1 mm into the upper endplate/vertebra, retaining the disc height (Fig. 1D). The surface of the bottom endplate was slightly reduced to fit the cage. Model 4 was prepared in the same manner as model 3, except that the cage height was increased to 6 mm. This equates to 3 mm of cage embedded within the upper endplate/vertebra (Fig. 1E). All endplates and interbody sites were maintained according to the intact Mimics model (Materialise) except at the C4C5 and C5C6 locations. Additionally, all surfaces and geometrics were set to minimize variability in interface interaction be-

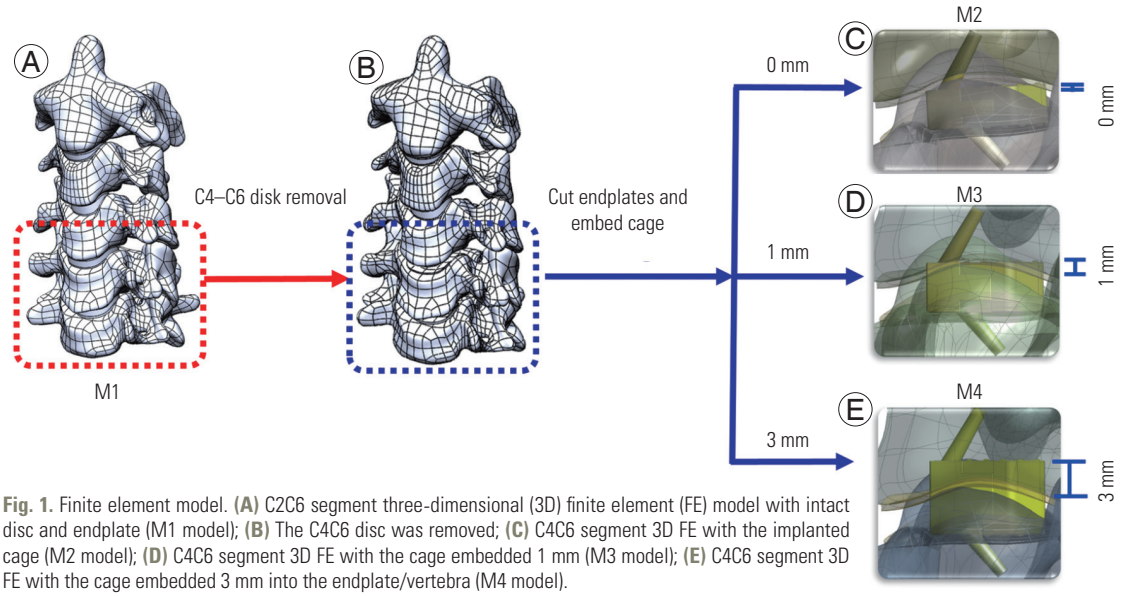

Fig. 1. Finite element model. **(A)** C2C6 segment three-dimensional (3D) finite element (FE) model with intact disc and endplate (M1 model); **(B)** The C4C6 disc was removed; **(C)** C4C6 segment 3D FE with the implanted cage (M2 model); **(D)** C4C6 segment 3D FE with the cage embedded 1 mm (M3 model); **(E)** C4C6 segment 3D FE with the cage embedded 3 mm into the endplate/vertebra (M4 model).

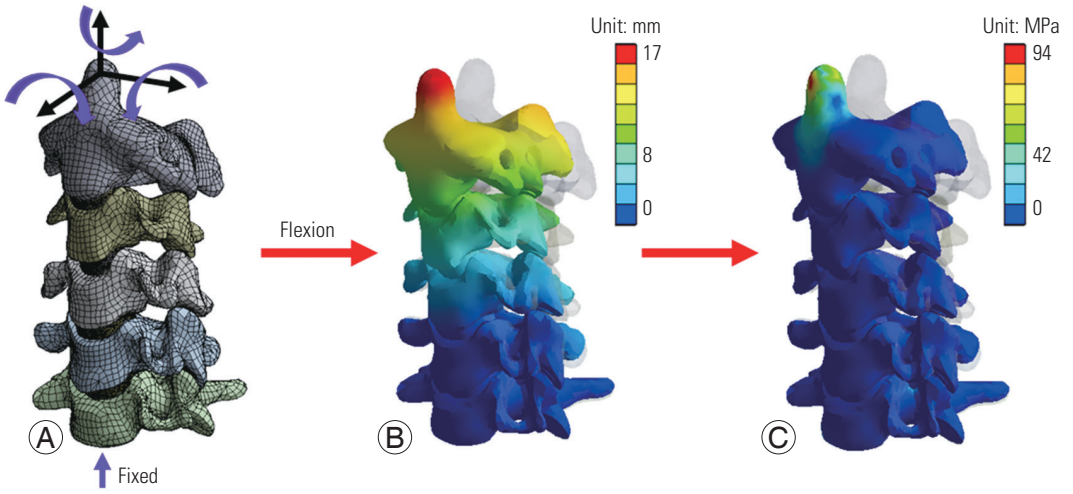

Fig. 2. (A) Meshing and load application of the finite element (FE) model; **(B)** displacement contour plot of the M1 model under 1 N·m of flexion; **(C)** von Mises stress contour plot of the M1 model under 1 N·m of flexion.

tween models (Fig. 1B). The C2C6 models were evaluated for flexion, extension, lateral bending, and axial rotation under a moment of 1 N·m (Fig. 2A). The meshing was validated using a convergence test. No significant difference was found among solutions. The practicality of the results was initially assessed using the typical deformation and von Mises stress of the whole model (Fig. 2A, C).

Maintenance of disc height during cage embedding is the most reasonable approach to maintain proper cervical alignment and minimize patient discomfort. The standard approach is to test a cage with a spacer to determine the disc height and select a cage that is a certain height taller than that. Although the capability of surface editing may not be as consistent in the endplate as it is in the cancellous bone, cuts made to the endplates were quite simple. As part of the surgical procedure in ACDF, the ALL and PLL were removed at the implant site within the finite element (FE) model.

Migration was defined as sliding on the contact surface between the cage and cancellous bone in M3 and M4. In M2, the measured contact surface was between the cage and the endplate. Subsidence was defined as the penetration of the cage body into the cancellous bone or endplate. The measured contact surface followed the same conventions applied to migration. Both results were collected directly from ANSYS Workbench (ANSYS Inc.) displace-

ment results.

ROM of the C3C4 and C4C5 segments in model 1 were compared to experimental data of cadaveric specimens and numerical reports of finite element analysis (FEA) in literature for validation of results. ROM and stress were observed in the upper vertebra and separately in C4C5 and C5C6 to examine the trends that would occur regarding implantation and prospective loads on adjacent intervertebral discs.

2. Material property

Material properties of the model were retrieved from literature shown in Table 1 (i.e., cortical bone, cancellous bone, intervertebral discs, and cartilage) [16,17]. Ligaments modeled as nonlinear springs with force–displacement were taken from literature shown in Fig. 3 [1]. The nucleus pulposus, annulus fibrosus, and all other components in this model were considered as elastic material [18,19]. The cage screws were assumed as titanium material.

Table 1. Material properties used in the model [1]

Component	Young's modulus (MPa)	Poisson ratio
Cortical bone	12,000	0.3
Cancellous bone	450	0.2
Endplate	500	0.4
Facet cartilage	10.4	0.4
Nucleus pulposus	1	0.49
Annulus fibrosus	50	0.45
Titanium Ti-6Al-4V (grade 5)	110,000	0.342
Tensile strength, ultimate	860	
Tensile strength, yield	790	

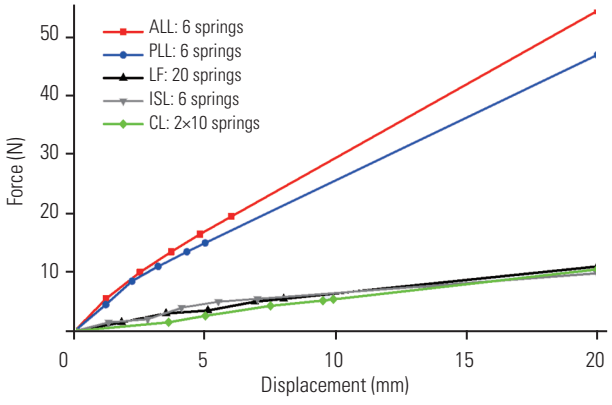

Fig. 3. All ligament force-displacement properties. ALL, anterior longitudinal; PLL, posterior longitudinal; LF, ligamentum flavum; ISL, interspinous ligament; CL, capsular ligament.

3. Boundary, contact, and loading conditions

The models were analyzed during natural spinal motions of flexion, extension, lateral bending, and axial rotation under ±1 N·m. The loading was applied to the tip of the C2 vertebral body and the bottom surface of the C6 vertebra was completely constrained (Fig. 2A). The contacts between natural components of the spine were considered as bonded (i.e., cancellous to cortical bone and endplates to annulus fibrosis). The facet joints were modeled as a gap with contact friction of 0.01 between facets. Contacts between the cage screws and the endplate were modeled with surface-to-surface contact elements with a frictional coefficient of 0.5 [20]. The contact between the cage screw/plate and cancellous bone was set at 0.95. All other contacts were set as bonded to simulate immediate postoperative conditions.

Results

1. Model validation

Our FE model (M1) was compared with experimental tests, *in vivo* or *in vitro*, and FE studies. The results are presented in Fig. 4A [19,21,22]. The von Mises stress and deformation of the C2–C6 specimen was recorded as a novel form of validation (Fig. 2B, C). Given that the model observed in this study does not match the usual vertebral range of C2–C6, it was determined that a more appropriate method would be to perform a comparison of the segmental ROM. The segmental ROM of the M1 model during flexion–extension, lateral bending, and axial rotation were all in the range of results observed in previous experiments and FE studies. The values recorded from the M1 model are well within the range of experimental outcomes. These comparisons validated this developed 3D FE model.

2. Range of motion

The ROM at the suggested ACDF site was compared in Fig. 4B to provide a better understanding of the maintenance of local alignment and the method of endplate

preparation. Under flexion, the natural spine (M1 model) rotated a total of about 16.8°. The implantation of cages in models M2–M4 reduced the ROM to 8° in M2, 8.5° in M3, and 8° in M4. Under 1 N·m of extension, the M1 model had a ROM of 17.4°. It was 7.4° in M2, 7.7° in M3, and 7.1° in M4. During bending, the ROM in the M1 model was about 22°. In M2 it was 7.2°. In M3, it was 7.5°. In M4, it was 6.8°. Under 1 N·m of torque, the M1 model experienced a ROM of 24.9°. The M2 model measured at 6° and the M3 and M4 models measured at 6.25° and 6.2°, respectively. The general convention that is maintained is equivalent flexion and extension capability, with slightly reduced bending and torque capabilities.

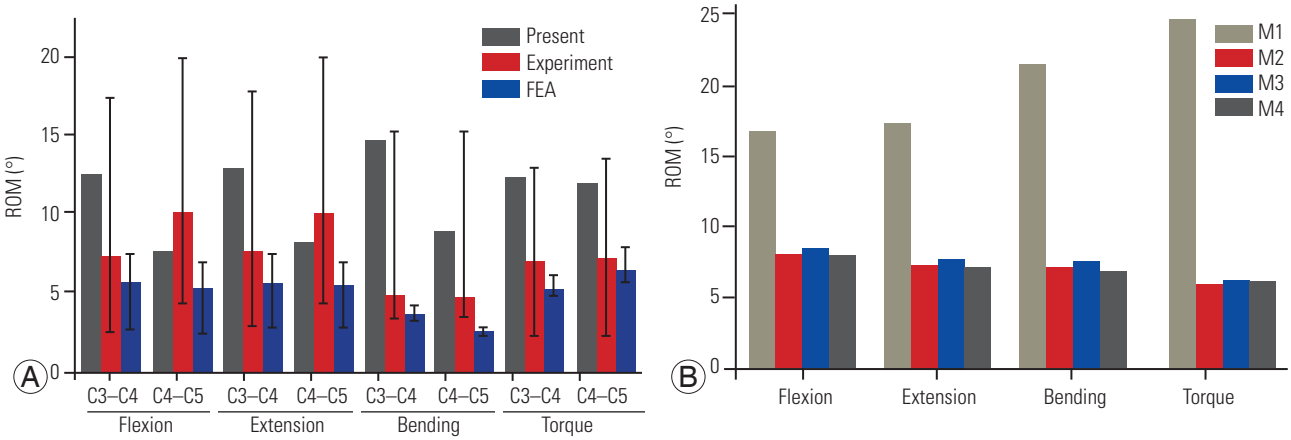

Fig. 4. (A) Our finite element (FE) model was compared with experimental tests (*in vivo* or *in vitro*), and existing FE studies; **(B)** C2C6 segmental range of motion (ROM) with M1, M2, M3, and M4 models. FEA, finite element analysis.

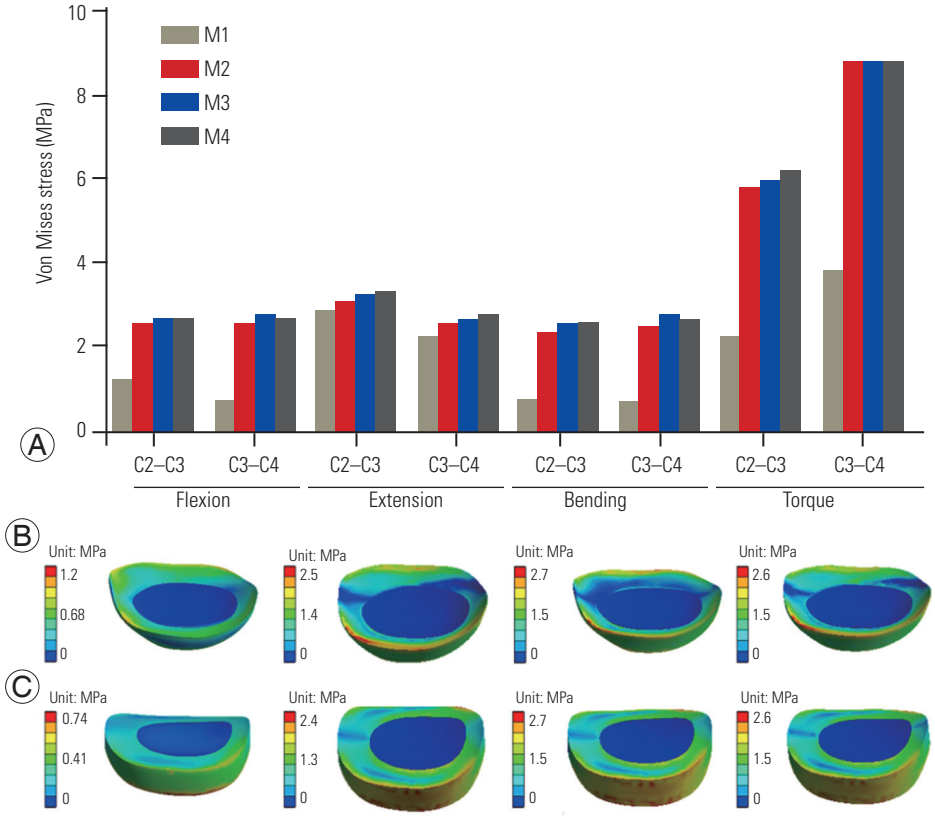

Fig. 5. (A) Comparison of maximum von Mises stress at the C2C3 and C3C4 disc with the M2, M3, and M4 models in the flexion, extension, lateral bending, and torque simulations; **(B)** von Mises stress in the C2C3 interbody disc during flexion for M2, M3, and M4 models from left to right; **(C)** von Mises stress in the C3C4 interbody disc during flexion for M2, M3, and M4 models from left to right.

3. Von Mises stress

Fig. 5A compares the maximum von Mises stress in the natural intervertebral discs, present at the C2C3 and C3C4 junctions. The maximum von Mises stress in the natural intervertebral discs increased as taller cages were embedded into the vertebra. Generally, the cages experienced greater stress in cases where the cages were embedded further into the vertebral body. Stress differences from model to model varied by approximately 6%. In all cases, the least stress was measured for the adjacent disks in the natural spine, M1 model. The maximum stress for all models took place in the C3C4 interbody disc during 1 N·m of torque. Two typical von Mises stress contours are shown in Fig. 5B and C. As shown, no significant difference was observed in the C3C4 interbody disc during flexion for the M2, M3, or M4 models.

4. Migration

Fig. 6 displays the comparison of the migration at the contact surface of the vertebra and the cage in the M2–M4 models. The results show that the migration at all contacts of C4C6 was the highest in the M4 model followed by the M2 model and finally the M3 model in all flexion, extension, lateral bending, and axial rotation simulations. The migrations created under extension moments were significantly less than other moments. In flexion, the migration at C4C5 was approximately 0.041 mm in the M2 model and reduced to 0.036 mm in the M3 model before increasing to 0.073 mm in the M4 model. Meanwhile, the migration at C5C6 endplates and the cage in the M3 model was still the lowest at approximately 0.045 mm, when compared with 0.051 mm in the M2 model and 0.055 mm in the M4 model. During lateral bending, the migration was slightly greater at C5C6 but significantly greater at C4C5. During axial rotation, the migration at C4C5 was the lowest of all groups. However, it was among the highest of all groups at C5C6. Maximum migration was predominantly found in the M4 model, whereas the least migration was consistently found in the M3 model.

5. Subsidence

Fig. 7 presents the subsidence at the contact surface between the endplates and cages in the M2–M4 models. The subsidence at all contacts of C4C6 during flexion, extension, lateral bending, and axial rotation simulations was always the highest in the M4 model. This is followed by the M2 model and then the M3 model. In all motions, the M2 model showed subsidence values at approximately 0.02 mm. The M3 model remained at approximately 0.015 mm. The subsidence in the M4 model showed an increase and had much greater variability at approximately 0.025

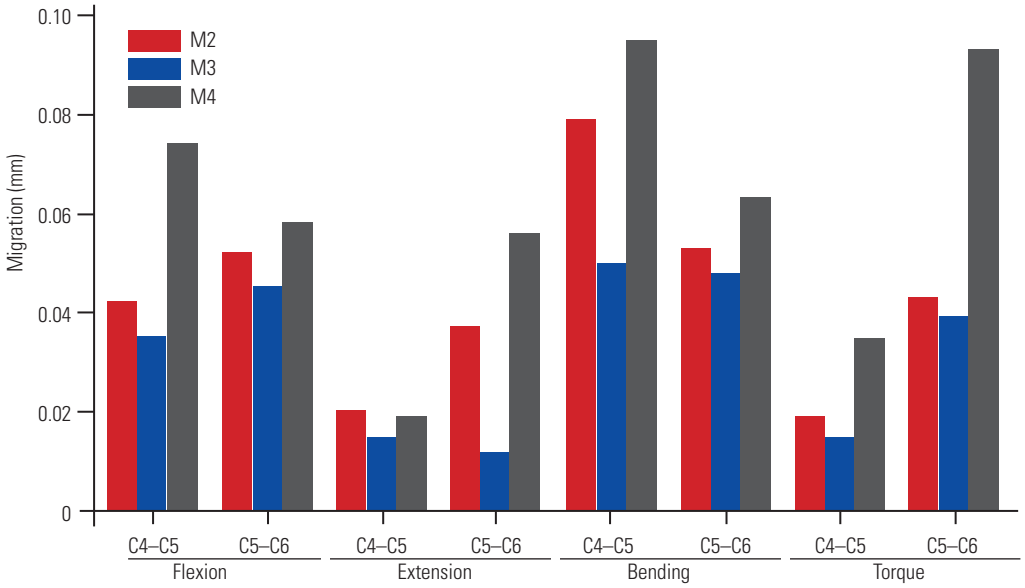

Fig. 6. Comparison of migration at the C4C5 and C5C6 junctions with the M2, M3, and M4 models in the flexion, extension, lateral bending, and torque simulations.

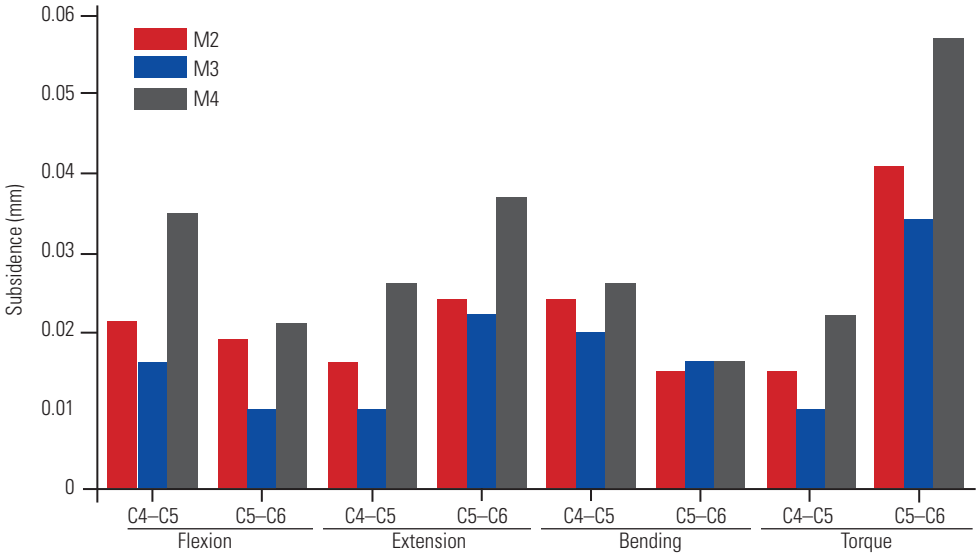

Fig. 7. Comparison of subsidence at the C4C5 and C5C6 junctions with the M2, M3, and M4 models in the flexion, extension, lateral bending, and torque simulations.

mm. Significant deviations from these values were only found in the torque simulations. The subsidence of the screws was higher in the case containing the tallest cage and most contact area with the cancellous bone.

Discussion

Published literature details the beneficial effects of the endplate on the biomechanical stability of the cervical spine [7,23]. Operating with only this information, one could conclude that any ACDF methodology that requires removal or significant editing of the vertebra would be inferior to the currently accepted method. The cartilaginous endplate is typically removed with the disc, leaving behind the vertebral endplate. This endplate has greater strength moduli than the underlying cancellous bone, making it the favorable contact for the cage. Another noted impact on the biomechanical stability of an implant is the contact area. The degree of contact with the underlying cancellous bone is greatly affected by friction. If the endplate is bypassed, more contact area is possible between the vertebra and the cage. Research shows that this higher contact area reduces the amount of migration and subsidence that occurs [24]. Reported subsidence and migration values were consistent with our study results [1]. The benefit of contact area weighed against the mechanical favorability of the endplate poses a question. Perhaps, a certain amount of contact area will lead to equivalent, if not decreased, subsidence and migration. The results of the M3 model make it apparent that considerable endplate removal can occur and provide less subsidence and migration. This is due to an increase in the contact area. In this study, subsidence and migration are defined using the entire contact that the cage has with the endplate and cancellous bone, where applicable. In the M2 model, the cage is inserted with minimal revision so that the only significant contact is with the vertebral endplate. Because of the concavity of the endplates, little contact is made at the top center face of the cage. In the M3 model, some of the contacts with the endplate are retained, providing some biomechanical stability. At this embedding depth, the entire top face of the cage makes contact with either the endplate or vertebra. Increasing beyond this point, as seen in the M4 model, greatly increases the subsidence and migration because the endplate's strength is completely nullified. A further embedding height may potentially make up for this loss, but a cage of that height would most likely become impractical for surgical methods as they would resemble an anterior cervical corpectomy and fusion procedure. Experimentally, the M3 model was the most biomechanically stable. Theoretically, it is the optimal scenario as well. The impact of the endplate strength is greater than the impact of the contact area. Thus, the intersection of these two opposing factors would be such that most of the vertebral endplate is preserved while giving full contact with the superior surface. Noteworthily, the FEA does not model the proposed scenario perfectly because partial removals have been known to have a slight impact on the overall

strength of the endplate. The exact value or method of determining this strength is not reported.

The practicality of significant endplate removal is limited by concavity. In the current model, only the superior surface is embedded because of its lower curvature. At the inferior surface, the ideal contact condition may be harder or even impossible to satisfy. The higher curvature means that more of the endplate will have to be removed to achieve a full contact area on the bottom surface of the cage. Additionally, the curvature of the endplate varies from patient to patient, so determining the success of this method must be evaluated individually.

Removal of the endplates tends to increase the stress experienced in adjacent healthy segments [25]. Considering this, in patients whose interbody discs are already degenerated, avoiding endplate removal may be beneficial as it will hold a greater portion of the load and have a lower long-term impact on those discs. This is apparent in the increasing stress trend as the cage is embedded further. Again, the M4 model showed the highest stress while the M2 model showed the least. The stress data of the upper vertebra intervertebral discs, namely, C2C3 and C3C4, indicate that the removal of endplate and cage embedding may increase the stress undergone in the adjacent vertebra. These greater stresses will speed up the disc degeneration rate and lead to ASD and increase the need for follow-up surgery for the affected segments.

One issue highlighted in the literature, regarding the endplate preparation, is the limitations of capability. Piezosurgery has been used to cleanly and effectively change the surface of the cortical bone as would be necessary in the case of complete endplate removal [26]. No comparably effective method exists for precise clearing of the endplates. However, one study demonstrated the feasibility of sound pressure signal auxiliary feedback in differentiating drilling conditions [27]. The common methodologies of endplate removal include the use of burrs, rasps, and curettes. It has been noted that these methods often fail to remove the endplates with precision in certain areas, leaving ridges and valleys that may affect the biomechanical behavior of the prosthesis [28]. Literature also shows that the thickness and strength of the endplates vary across the transverse plane [29]. An in-depth review and study on the localized tendencies of subsidence would be beneficial to determine the feasibility of endplate removal in only certain areas. This, however, would require investigation for effectiveness and potential drawbacks of having unnatural, nonuniform endplate thickness during ACDF.

Conclusions

The postoperative stability of the cage is important to the alignment of the cervical spine and the maintenance of intervertebral disc height. In this study, four FEA models were conceived and tested under 1 N·m of flexion, extension, lateral bending, and torque. Our FEA results were validated using comparisons of the M1 model with the values presented in the literature with similar conditions. The choice of endplate preparation created a loss of intact ROM in the C4C6 segments, ranging from 53% to 76%. Beyond the initial difference between the M1 model and the M2 model, the significance of ROM changes decreases drastically. Endplate preparation caused negligible stress differences in the healthy intervertebral discs above the ACDF site. Once the full contact area was obtained, the strength difference caused more subsidence and migration to take place as more of the endplate was removed. Based on the data of this FEA, partial removal of the endplate is often the most viable option. However, the stresses exerted on the adjacent discs should be heeded as a danger for patients with lower biomechanical integrity (i.e., patients with osteoarthritis/osteoporosis and older patients). A 1 mm embedding depth seems to be the best balance of mechanical strength and contact area, resulting in the most favorable stability. The ideal embedding depth should vary between individuals on the basis of the concavity of their endplates. Further studies are recommended to outline a methodology for determining the ideal embedding height from patient to patient and to develop a more efficient way of preparing the endplates and vertebral body.

Conflict of Interest

No potential conflict of interest relevant to this article was reported.

Acknowledgments

This is a finite element analysis study. No clinical samples or data were included in this paper. This research was supported by the Boca Raton Regional Hospital Foundation (award # SP 19-579).

Author Contributions

Data acquisition: ML; analysis of data: ML; drafting of the manuscript: ML; conception and design: ML; critical revision: ML, RP, SP, EE, CT, FV; administrative support: CT, FV; and supervision: CT, FV.

References

1. Lin M, Shapiro SZ, Doulgeris J, Engeberg ED, Tsai CT, Vrionis FD. Cage-screw and anterior plating combination reduces the risk of micromotion and subsidence in multilevel anterior cervical discectomy and fusion: a finite element study. Spine J 2021;21:874-82.
2. Jagannathan J, Shaffrey CI, Oskouian RJ, et al. Radiographic and clinical outcomes following single-level anterior cervical discectomy and allograft fusion without plate placement or cervical collar. J Neurosurg Spine 2008;8:420-8.
3. Barsa P, Suchomel P. Factors affecting sagittal malalignment due to cage subsidence in standalone cage assisted anterior cervical fusion. Eur Spine J 2007;16:1395-400.
4. Fujibayashi S, Neo M, Nakamura T. Stand-alone interbody cage versus anterior cervical plate for treatment of cervical disc herniation: sequential changes in cage subsidence. J Clin Neurosci 2008;15:1017-22.
5. Gercek E, Arlet V, Delisle J, Marchesi D. Subsidence of stand-alone cervical cages in anterior interbody fusion: warning. Eur Spine J 2003;12:513-6.
6. Hakalo J, Wronski J, Ciupik L. Subsidence and its effect on the anterior plate stabilization in the course of cervical spondylodesis. Part I: definition and review of literature. Neurol Neurochir Pol 2003;37:903-15.
7. Okano I, Jones C, Salzmann SN, et al. Endplate volumetric bone mineral density measured by quantitative computed tomography as a novel predictive measure of severe cage subsidence after standalone lateral lumbar fusion. Eur Spine J 2020;29:1131-40.
8. Dunn RN, Pretorius C. Cervical PEEK cage standalone fusion: the issue of subsidence. SA Orthop J 2011;10:25-9.
9. Lee DH, Cho JH, Hwang CJ, et al. What is the fate of pseudarthrosis detected 1 year after anterior cervical discectomy and fusion? Spine (Phila Pa 1976) 2018;43:E23-8.
10. Fraser JF, Hartl R. Anterior approaches to fusion of the cervical spine: a metaanalysis of fusion rates. J Neurosurg Spine 2007;6:298-303.
11. Lou J, Liu H, Rong X, Li H, Wang B, Gong Q. Geometry of inferior endplates of the cervical spine. Clin Neurol Neurosurg 2016;142:132-6.
12. El Baz EA, Sultan AM, Barakat AS, Koptan W, ElMiligui Y, Shaker H. The use of anterior cervical interbody spacer with integrated fixation screws for management of cervical disc disease. SICOT J 2019;5:8.
13. Ng EP, Yip AS, Wan KH, et al. Stand-alone cervical cages in 2-level anterior interbody fusion in cervical spondylotic myelopathy: results from a minimum 2-year follow-up. Asian Spine J 2019;13:225-32.
14. Cheng CC, Ordway NR, Zhang X, Lu YM, Fang H, Fayyazi AH. Loss of cervical endplate integrity following minimal surface preparation. Spine (Phila Pa 1976) 2007;32:1852-5.
15. Bydon M, Xu R, Macki M, et al. Adjacent segment disease after anterior cervical discectomy and fusion in a large series. Neurosurgery 2014;74:139-46.
16. Clausen JD, Goel VK, Traynelis VC, Scifert J. Uncinate processes and Luschka joints influence the biomechanics of the cervical spine: quantification using a finite element model of the C5-C6 segment. J Orthop Res 1997;15:342-7.
17. Ha SK. Finite element modeling of multi-level cervical spinal segments (C3-C6) and biomechanical analysis of an elastomer-type prosthetic disc. Med Eng Phys 2006;28:534-41.
18. Panzer MB, Cronin DS. C4-C5 segment finite element model development, validation, and load-sharing investigation. J Biomech 2009;42:480-90.
19. Hua W, Zhi J, Wang B, et al. Biomechanical evaluation of adjacent segment degeneration after one- or two-level anterior cervical discectomy and fusion versus cervical disc arthroplasty: a finite element analysis. Comput Methods Programs Biomed 2020;189:105352.
20. Polikeit A, Ferguson SJ, Nolte LP, Orr TE. Factors influencing stresses in the lumbar spine after the insertion of intervertebral cages: finite element analysis. Eur Spine J 2003;12:413-20.
21. Lee SH, Im YJ, Kim KT, Kim YH, Park WM, Kim K. Comparison of cervical spine biomechanics after fixed- and mobile-core artificial disc replacement: a finite element analysis. Spine (Phila Pa 1976) 2011;36:700-8.
22. Barker JB, Cronin DS, Nightingale RW. Lower cervical

spine motion segment computational model validation: kinematic and kinetic response for quasi-static and dynamic loading. J Biomech Eng 2017;139:061009.
23. Mabe I, Goswami T. Finite element analysis of superior C3 cervical vertebra endplate and cancellous core under static loads. J Biomed Eng Biosci 2016;3:26-33.
24. Calvo-Echenique A, Cegonino J, Chueca R, Perez-Del Palomar A. Stand-alone lumbar cage subsidence: A biomechanical sensitivity study of cage design and placement. Comput Methods Programs Biomed 2018;162:211-9.
25. Pinder EM, Sharp DJ. Cage subsidence after anterior cervical discectomy and fusion using a cage alone or combined with anterior plate fixation. J Orthop Surg (Hong Kong) 2016;24:97-100.
26. Pan SF, Sun Y. Application of piezosurgery in anterior cervical corpectomy and fusion. Orthop Surg 2016;8:257-9.
27. Shao F, Tang M, Bai H, Xue Y, Dai Y, Zhang J. Drilling condition identification based on sound pressure signal in anterior cervical discectomy surgery. Med Sci Monit 2019;25:6574-80.
28. Lim TH, Kwon H, Jeon CH, et al. Effect of endplate conditions and bone mineral density on the compressive strength of the graft-endplate interface in anterior cervical spine fusion. Spine (Phila Pa 1976) 2001;26:951-6.
29. Pitzen T, Schmitz B, Georg T, et al. Variation of endplate thickness in the cervical spine. Eur Spine J 2004;13:235-40.